A SECOND-ORDER BPF USING A MINIATURIZED-ELEMENT FREQUENCY SELECTIVE SURFACE

O. Manoochehri[*], S. Abbasiniazare, A. Torabi, and K. Forooraghi

Faculty of Electrical and Computer Engineering, Tarbiat Modares University, Nasr Bridge, Tehran, Iran

Abstract—A new type of low-profile frequency selective surface (FSS) with an overall thickness of $\lambda/40$ and a second-order band pass frequency response is presented. The proposed FSS is composed of two metal layers, separated by a thin dielectric substrate. Each layer is a two-dimensional periodic structure with sub-wavelength periodic unit cells. By printing the same topology on each side of the substrate, a second-order frequency response is realized. To provide a physical insight into the operating mechanism, equivalent circuit networks are also investigated in each step of design procedure. Using the proposal technique, low profile and reduced sensitivity to angle of incident wave for both TE and TM polarizations are obtained and the overall thickness of the substrate is fairly thin. FSS samples are designed, fabricated, and installed in waveguide operating at X-band and a good agreement between the simulated and measured results is achieved.

1. INTRODUCTION

Frequency selective surfaces (FSSs) structures are regarded as the free space counterparts of microwave filters [1]. A typical FSS structure consists of an array of patches printed on a thin dielectric layer [2–4]. The transmit- and reflect-band frequencies depend on the patch and unit cell size. A complementary structure with apertures on the conductor is also used as an FSS [5]. The FSS structures are commonly used as antenna radomes to eliminate undesired frequency components. They are also used in dual-band Cassegrain reflector systems [6, 7]. The principle of operation of an FSS is very similar to that of a waveguide filter. An infinite array of conducting patches

is equivalent to a shunt susceptance in response to a plane wave incidence. Operation of a single-layer FSS relies on the magnitude of the susceptance that is a function of the operating frequency. A transmit band exists if the susceptance has a small magnitude that would allow signal transmission.

A high susceptance yields a reflect band. In a multilayer FSS the separating distances between the layers also play an important role in determining the transmit/reflect-band frequencies [8]. In traditional FSSs such as resonant dipoles of different shapes [9], and Jerusalem cross [10] and resonant loop, the unit cells inter element spacing generally correspond to half a wavelength at the desired frequency of operation. Recently a new method for designing frequency-selective surfaces has been proposed in [11] and further developed in [12, 13]. Instead of using resonant structures special sub-wavelength unit cells are employed. In this paper, a new type of sub-wavelength miniaturized-element frequency selective surface (MEFSS) is presented. Initially, a first order bandpass FSS is designed using metallic square loops and wire grids which are printed on the same side of an electrically thin substrate. The order of the response could be increased by cascading two or more layers of FSS, to achieve a higher order bandpass response. Each side of FSS represents a band-pass LC circuit and act as a first-order band-pass filter. The separation distance between the two FSS surfaces, (unlike traditional FSSs) can also be miniaturized. Comparing the proposed FSS with structure in [14–16], the distances between the unit cells are reduced by an amount of approximately 40% leading to a significant reduction of sensitivity to the incidence angle.

2. FSS DESIGN

Figure 1 demonstrates the prototype of the first-order bandpass Miniaturized-Element FSS (MEFSS). This FSS structure consists of metallic square loops and a wire grid etched on the same side of a Taconic RF-35 substrate with $\varepsilon_r = 3.5$, $\tan \delta = 0.0018$. This first-order band-pass FSS has a single metal layer supported by an electrically thin dielectric substrate. The thickness of the substrate is $h = 0.762 \, \text{mm}$.

Unit cell of this two dimensional periodic structure is depicted in Figure 2. The periodicity distance of the unit cells in both x and y directions are D. It is observed that the structure is symmetric with respect to x and y axes. Table 1 demonstrates the optimized parameters values of a unit cell. The equivalent circuit model for the square loop array is a series LC circuit [17, 18]. The inductive part (L_g) of this model is produced by the strips on each side, whereas the
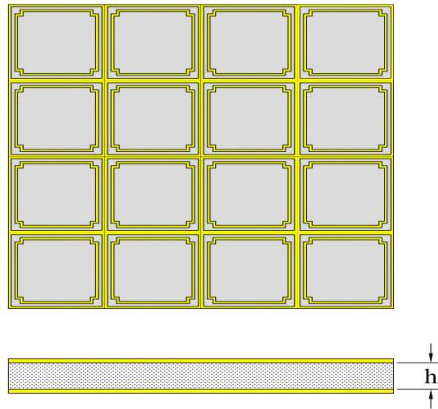
Figure 1. Top and side views of the bandpass MEFSS etched on the two side of a Taconic RF-35 dielectric substrate with the characteristics of $\varepsilon_r = 3.5$, $\tan\delta = 0.0018$ and thickness of $h = 0.762\,\mathrm{mm}$.
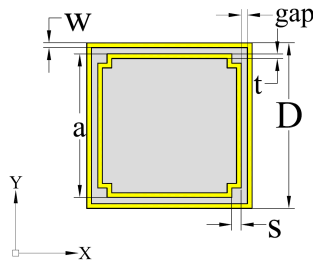
Figure 2. The unit cell of the FSS shown in Figure 1. Each unit cell is composed of a single LC loop inside a section of the mesh grid. The structure is designed to be polarization insensitive at normal incidence.

capacitive component (C_1) is created by the short gaps located between the loops and the wire grids. Moreover, due to the presence of the wire grid in the vicinity of the loop array, this series LC circuit will parallel with another inductive element L_g. The dielectric substrate and free space on both sides of the MEFSS are modeled by transmission line lengths. The characteristic impedance and the length of the substrate transmission lines are represented by $Z_1 = Z_0/\sqrt{\varepsilon_r}$ and, h (substrate thickness), respectively. The equivalent circuit model of the first order bandpass MEFSS is presented in Figure 3(a). This equivalent circuit is composed of quasi-lumped capacitors and inductors. Each transmission line can be modeled by lumped elements as indicated in Figure 3(b) [19]. In this model, dielectric and Ohmic losses are
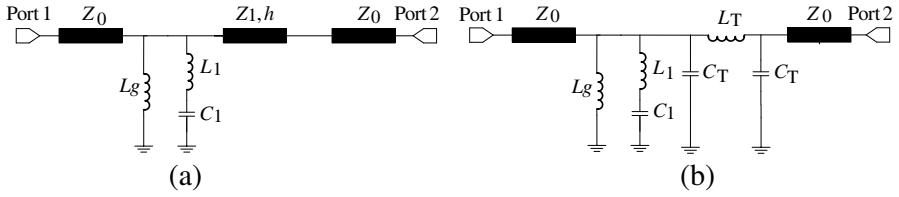
Figure 3. The equivalent circuit model for (a) the first-order bandpass MEFSS and (b) first-order bandpass MEFSS and dielectric substrate for normal incident waves. L_g is the wire grid inductances, C_T and L_T model the dielectric substrate [19].

Table 1. Physical parameters and dimensions of two order bandpass presented in Figure 2.

Parameter	D	a	w	s
Value	5.3 mm	4.6 mm	0.15 mm	0.3 mm
Parameter	t	h	ε_r	—
Value	0.15 mm	0.762 mm	3.5	—

ignored. The series inductance L_T and shunt capacitance C_T are used as equivalent model of the transmission line (dielectric substrate). Both of the equivalent circuit models of this MEFSS have been analyzed using the ADS simulation platform and the results are presented in Figure 4.

Also, this figure illustrates the full-wave simulations preformed by CST. In Table 2 equivalent values are presented. These values are achieved in order to exhibit a first-order band-pass frequency response that conforms well with full-wave simulations. The full wave simulation is performed regarding the normal incident wave angle. Also, the equivalent circuit model described by Figures 3(a) and 3(b) is only valid for normal incident waves. As observed from Figure 4, a null is achieved near 12 GHz. Which corresponds to the short circuit frequency of the series $L_1 C_1$ ($f_{\text{null}} \approx 1/2\pi\sqrt{L_1 C_1}$ at about 12.3 GHz). As mentioned earlier, the series LC circuit is the equivalent circuit model for the square loop array.

The frequency response of the series LC exhibits a band-stop feature. Through the addition of the wire grid (L_g inductance) in the gap between the square loops, a null will appear at low frequencies. Therefore, the MEFSS depicted in Figure 2 demonstrates a first-order bandpass frequency characteristic. Here, the transmission line model
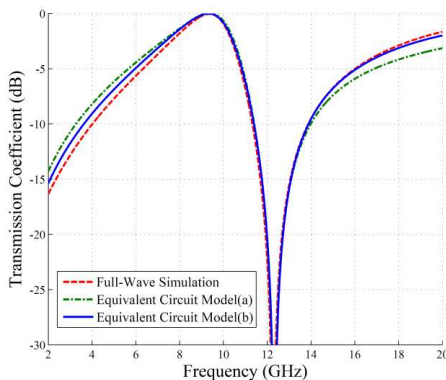
Figure 4. Transmission Coefficients of the MEFSS depicted in Figure 2. ADS is employed for the simulation of equivalent circuit model shown on Figure 3, where the element values are according to the Table 2.

Table 2. Equivalent values for two model presented in Figure 3.

Parameter	C_1 (fF)	L_1 (nH)	L_g (nH)	C_T (fF)	L_T (nH)
3(a) model	40.55	4.12	2.89	—	—
3(b) model	42.5	3.923	2.52	11.64	0.963

(C_T and L_T) can be neglected due to their insignificant values; the passband frequency of the MEFSS can be derived using a simple circuit analysis as

$$f_p \approx 1/2\pi\sqrt{(L_g + L_1)C_1} \tag{1}$$

which is found to be $f_p \approx 9.44$ GHz. C_T and L_T values can be extracted from the following formulas [19]:
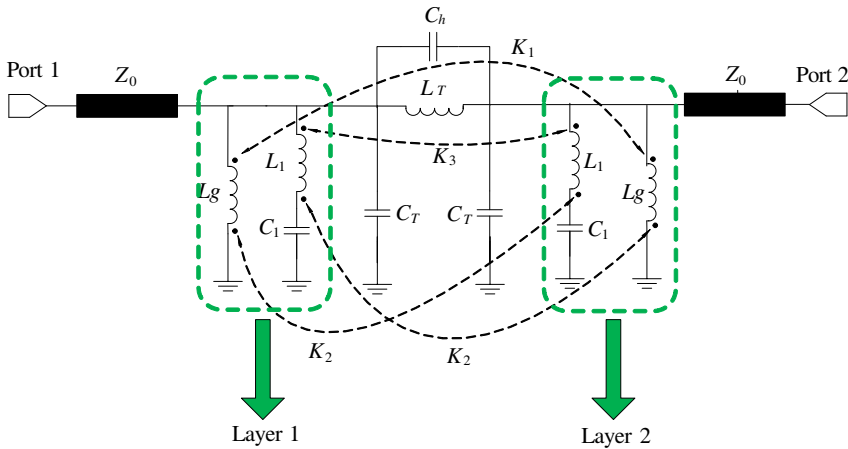
$$L_T = \frac{Z_1}{\omega}\sin(\beta h) \tag{2}$$

$$C_T = \frac{1}{Z_1\omega}\tan\left(\frac{\beta h}{2}\right)' \tag{3}$$

The above equations are solved for L_T and C_T, with the values listed in Table 2. As can be seen, the resulting values are insignificant.

Also L_g is obtained by [20]

$$L_g = \mu_0\mu_{eff}\frac{D}{2\pi}\ln\left(\frac{1}{\sin\left(\frac{\pi w}{D}\right)}\right) \tag{4}$$

Figure 5. The equivalent circuit model for the second-order bandpass MEFSS.

where β is the dielectric phase constant, h the dielectric substrate thickness, D the period of the structure, μ_0 the free space permeability, μ'_{eff} the effective permeability, and w the half of strip width.

As can be seen from Table 2, there is a good agreement between the extracted model parameters and corresponding formulas. The second step of the design procedure is realization of a second-order frequency response without increasing the MEFSS size. Similar to the traditional FSS, it is necessary to cascade two identical first-order FSSs. Unlike the conventional FSS which needs quarter wavelength spacing between FSS panels in order to realize a second-order bandpass FSS, we have printed two panels of first-order band-pass FSSs on two sides of the same substrate with $h = 0.762$ mm. Using this technique, a second-order ultra low-profile band-pass MEFSS is obtained. The equivalent circuit model for the second-order bandpass MEFSS may be achieved by extending the model presented in Figure 3. As the second MEFSS panel is printed on the other side of the substrate, it is necessary to duplicate the equivalent circuit of the MEFSS panel along the transmission line model elements of the previous panel (as shown in Figure 5). Besides, it is necessary to add another capacitance between the two panels to model the electric interaction between the layers. An inductance is also considered in order to model the magnetic interaction between the layers.

The transmission coefficient of the second-order dual-band MEFSS is calculated by both methods (equivalent circuit model by ADS and full wave simulation by CST), and presented in Figure 6. Which shows a very good agreement between the results. The element
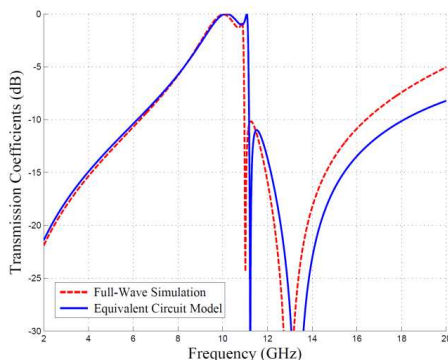
Figure 6. Transmission coefficient of the second-order bandpass MEFSS. Full-wave simulation by CST and equivalent circuit analyzed by ADS (Figure 5), where the element values are according to the Table 3.

**Table 3.** Equivalent values for second-order bandpass presented in Figure 5.

Parameter	C_1 (fF)	L_1 (nH)	L_g (nH)	C_T (fF)	L_T (nH)
value	40.55	4.12	2.52	11.64	0.963
Parameter	K_1	K_2	K_3	C_h (fF)	—
value	0.15	0.15	-0.076	30	—

values are provided in Table 3.

Figures 7(a), 7(b) show the transmission coefficients of the FSS when a transverse electric (TE) and magnetic (TM) polarization wave is incident upon its surface with different angles of incidence, respectively ($\theta = 0°$ represents the normal incidence). The FSS response does not significantly change for incidence angles in the range of $\pm 60°$ off bore-sight. At normal incidence, the two polarizations have exactly the same response, since the FSS structure is rotationally symmetric. As the angle of incidence increases, however, the response of the structure for the two different polarizations will change. For the TE incidence, as the angle of incidence changes, the wave impedance varies as following equation:

$$Z_{\text{TE}} = \frac{Z_0}{\cos \theta} \tag{5}$$

Therefore, for large incidence angles, the loaded quality factor of the parallel resonators of Figure 5 increases or equivalently the bandwidth of each resonator decreases. This is evident from Figure 7(a), where the
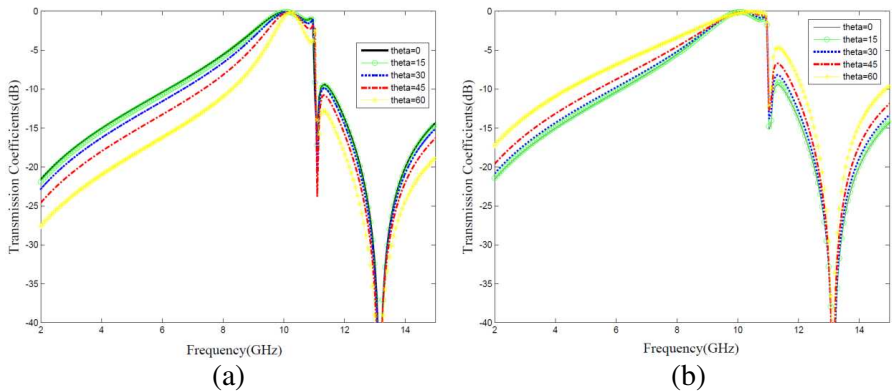
Figure 7. Transmission coefficient of the second-order bandpass MEFSS full-wave simulation by CST for various angles of incidence. (a) TE and (b) TM polarization.

FSS bandwidth corresponding to each transmission pole is reduced and consequently the pass-band ripple is increased. The wave impedance for the TM polarization, however, varies as following equation:

$$Z_{\text{TM}} = Z_0 \cos \theta \tag{6}$$

Therefore, for large incidence angles, decreases in the TM mode resulting in the broadening of the FSS bandwidth as observed from Figure 7(b). The unit cell dimensions of the FSS are $Dx = Dy = D = 5.3\,\text{mm}$, which is slightly smaller than $\lambda_0/5$, where λ_0 is the free space wavelength at $10\,\text{GHz}$. To further reduce the sensitivity of the response of the FSS to the angle of incidence, the unit cell size of the FSS can further be miniaturized. This is accomplished by reducing the unit cell dimensions while maintaining the effective capacitance and inductance values. If the unit cell size, D, is decreased, the capacitance value can be maintained by decreasing the spaces between the rings, or increasing the effective side length of the capacitor. Decreasing the spacing is feasible in theory but is limited by fabrication techniques used.

3. EXPERIMENTAL VERIFICATION AND MEASUREMENT RESULTS

In order to avoid errors in the frequency response characterization of the FSSs, arising from the edge diffraction, the general approach is to use a metallic waveguide suitable for the desired band. Following the same approach, a section of FSS, almost equivalent to eight unit cells

of proposed FSS, are enclosed inside a rectangular waveguide and the corresponding frequency response is measured. The advantage of this method is that the waveguide presents an enclosed environment which can be measured with high accuracy. For this purpose, the setup of Figure 8 is employed. A WR-90 waveguide is used and FSS section is placed inside the waveguide. The equivalent circuit of the element embedded in waveguide is parallel combination of an inductor and a series LC that are separated by a short length of transmission line.

In this case, however, it is important to notice that Z_0 and Z_1, as shown in Figure 3(a) or Figure 5, must be replaced with Z_{0TE10} and Z_{1TE10}, where Z_{0TE10} and Z_{1TE10} are the TE_{10} mode impedances of the air-filled waveguide and the dielectric, respectively. Nevertheless the TEM plane waves used in the simulation of infinite FSS structures are inaccurate in this case; because the WR-90 waveguide does not support a single TEM wave and the simulated results do not provide the response at normally incident TEM wave, but they typically demonstrate the frequency response of the second-order FSS at oblique incidence illuminated by two plane waves. This structure can be regarded as a second-order bandpass waveguide filter. A good agreement is, however, obtained between the predicted and measured results which validates the design methodology and accuracy of the simulation results. The frequency response of this second-order waveguide filter is simulated using HFSS and its response is measured using the setup shown in Figure 8. The measured and simulated results are presented in Figure 9, and a very good agreement. The measurement results show that FSS waveguide filter has an insertion loss of 0.5 dB, which is mainly attributed to Ohmic and dielectric losses of structure. The minor discrepancies might be ascribed to fabrication tolerance in the implementation and assembly of the FSS section into the waveguide.
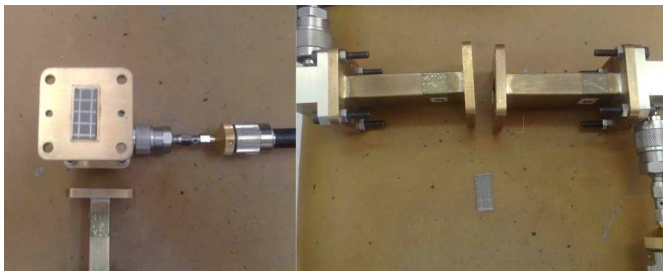
Figure 8. Setup for measuring the response of the FSS, piece of FSS is placed inside a WR-90 waveguide.
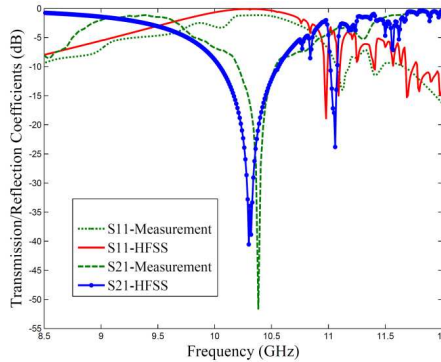
Figure 9. Measured and simulated transmission/reflection coefficients of the test sample of the FSS. Simulations are performed by HFSS.

4. CONCLUSION

In this paper, a frequency selective surface with miniaturized elements is presented. These elements can be used in low power waveguide filters. A new technique was adopted to achieve second-order bandpass responses using low-profile configurations. Resonant elements are, unlike the traditional FSSs that make use of resonant dipoles or slot structures, made up of two layers of spatial quasi-lumped elements.

The principles of operation of FSS along with measurement results of the typical structure are demonstrated, and validity of the design method is confirmed. The proposed structure exhibits lower sensitivity to the incidence angle than the traditional ones.

ACKNOWLEDGMENT

REFERENCES

1. Munk, B., *Frequency Selective Surfaces: Theory and Design*, John Wiley & Sons, New York, 2000.

2. Islam, S., J. Stiens, G. Poesen, R. Vounckx, J. Peeters, I. Bogaert, D. De Zutter, and W. De Raedt, "Simulation and experimental verification of W-band finite frequency selective surfaces on infinite background with 3D full wave solver nspwmlfma," *Progress In Electromagnetics Research*, Vol. 101, 189–202, 2010.

3. Zhang, J.-C., Y.-Z. Yin, and J.-P. Ma, "Design of narrow band-pass frequency selective surfaces for millimeter wave applications," *Progress In Electromagnetics Research*, Vol. 96, 287–298, 2009.

4. Martinez-Lopez, R., J. Rodriguez-Cuevas, A. E. Martynyuk, and J. I. Martinez Lopez, "An active ring slot with RF MEMS switchable radial stubs for reconfigurable frequency selective surface applications," *Progress In Electromagnetics Research*, Vol. 128, 419–440, 2012.

5. Munk, B., *Finite Antenna Arrays and FSS*, Wiley-Interscience, New York, 2003.

6. Huang, J., T. Wu, and S. Lee, "Tri-band frequency selective surface with circular ring elements," *IEEE Trans. on Antennas and Propagat.*, Vol. 42, 166–175, 1994.

7. Li, H., B.-Z. Wang, G. Zheng, W. Shao, and L. Guo, "A reflectarray antenna backed on FSS for low RCS and high radiation performances," *Progress In Electromagnetics Research C*, Vol. 15, 145–155, 2010.

8. Lima, A. C. D. C. and E. A. Parker, "Fabry-Perot approach to the design of double layer FSS," *IEEE Proc. Microwave Antennas Propagat.*, Vol. 143, 157–162, 1996.

9. Munk, B., R. Kouyoumjian, and L. Peters, Jr., "Reflection properties of periodic surfaces of loaded dipoles, *IEEE Trans. on Antennas and Propagat.*, Vol. 19, 612–617, Sep. 1971.

10. Monavar, F. M. and N. Komjani, "Bandwidth enhancement of microstrip patch antenna using Jerusalem cross-shaped frequency selective surfaces by invasive weed optimization approach," *Progress In Electromagnetics Research*, Vol. 121, 103–120, 2011.

11. Sarabandi, K. and N. Behdad, "A frequency selective surface with miniaturized elements," *IEEE Trans. on Antennas and Propagat.*, Vol. 55, 2007.

12. Behdad, N. and M. Al-Joumayly, "A low-profile third-order band-pass frequency selective surface," *IEEE Trans. on Antennas and Propagat.*, Vol. 57, 2009.

13. Teo, P., et al., "Frequency-selective surfaces for GPS and DCS1800 mobile communication. 1. Quad-layer and single-layer FSS design," *Microwaves, Antennas & Propagation, IET*, Vol. 1, 314–321, 2007.

14. Behdad, N., A second-order band-pass frequency selective surface using nonresonant subwavelength periodic structure, *Microwave Opt. Technol. Lett.*, Vol. 50, 1639–1643, 2008.

15. Pirhadi, A., et al., "Analysis and design of dual band high directive

EBG resonator antenna using square loop FSS as superstrate layer," *Progress In Electromagnetics Research*, Vol. 70, 1–20, 2007.

16. Guo, C., et al., "A novel dualband frequency selective surface with periodic cell perturbation," *Progress In Electromagnetics Research B*, Vol. 9, 137–149, 2008.

17. Gustafsson, M. and S. Nordebo, "Bandwidth, *Q* factor, and resonance models of antennas," *Progress In Electromagnetics Research*, Vol. 62, 1–20, 2006.

18. Langley, R. J. and E. A. Parker, "Equivalent-circuit model for arrays of square loops," *Electron. Letters*, Vol. 18, 294–296, 1982.

19. Pozar, D., *Microwave Engineering*, John Wiley & Sons, Wiley, New York, 2008.

20. Marcuvitz, N., *Waveguide Handbook*, Boston Technical Publishers, Lexington, MA, 1964.